Electronic Supporting Information

Non-equivalent Mn^{4+} doping into A_2NaScF_6 (A = K, Rb, Cs) hosts toward short fluorescence lifetime for backlight display application

Y. Y. Zhou [a], E. H. Song [a], M. G. Brik [bcd], Y. J. Wang [a], T. Hu [a], Z. G. Xia [a] and Q. Y. Zhang [a]*

[a] State Key Laboratory of Luminescent Materials and Devices, South China University of Technology, Guangzhou, 510641, P. R. China.

[b] College of Science, Chongqing University of Posts and Telecommunications, Chongqing, 400065, P. R. China.

[c] Institute of Physics, University of Tartu, W. Ostwald Str 1, Tartu, 50411, Estonia.

[d] Institute of Physics, Jan Długosz University, Armii Krajowej 13/15, PL-42200 Częstochowa, Poland.

*Corresponding author E-mail: qyzhang@scut.edu.cn

1. Crystal field calculations

The energy levels of impurity ions with an unfilled d-shell in a crystal field (CF) of arbitrary symmetry can be calculated by diagonalizing the following CF Hamiltonian in the framework of the exchange charge model (ECM) of crystal field: [1]

$$H = \sum_{p=2,4} \sum_{k=-p}^{p} B_p^k O_p^k \tag{1}$$

where O_p^k are the linear combinations of the irreducible tensor operators acting on the angular parts of the impurity ion's wave functions, and B_p^k are the crystal field parameters (CFPs), which can be calculated from the crystal structure data. The Hamiltonian (1) is

defined in the space spanned by all wave functions of the free ion's LS terms (which arise due to the Coulomb interaction between electrons of an impurity ion). In ECM the CFPs are expressed as a sum of two terms :[1]

$$B_p^k = B_{p,q}^k + B_{p,S}^k \tag{2}$$

with

$$B_{p,q}^k = -K_p^k e^2 \left\langle r^p \right\rangle \sum_i q_i \frac{V_p^k(\theta_i, \varphi_i)}{R_i^{p+1}} \tag{3}$$

and

$$B_{p,S}^k = K_p^k e^2 \frac{2(2p+1)}{5} \sum_i \left(G_s S(s)_i^2 + G_\sigma S(\sigma)_i^2 + \gamma_p G_\pi S(\pi)_i^2 \right) \frac{V_p^k(\theta_i, \varphi_i)}{R_i} \tag{4}$$

The first term $B_{p,q}^k$ describes the point charge contribution to the CFPs, which arises from the electrostatic interaction between the central ion and the lattice ions enumerated by index *i* with charges q_i and spherical coordinates, R_i, θ_i, φ_i. The averaged values $\left\langle r^p \right\rangle$, where *r* is the radial coordinate of the *d* electrons of the optical center (they are also called the moments of the 3d electron density), can be obtained either from the literature or calculated numerically, using the radial parts of the corresponding ion's wave functions. The values of the numerical factors K_p^k, γ_p, the expressions for the polynomials V_p^k and the definitions of the operators O_p^k can all be found in Ref. [1] and thus are not shown here for the sake of brevity.

The second term of Eq. (2) $B_{p,S}^k$ is proportional to the overlap between the wave functions of the central ion and ligands and thus includes all covalent effects. The $S(s), S(\sigma), S(\pi)$ terms correspond to the overlap integrals between the *d*-functions of the central ion and *p*- and *s*-functions of the ligands: $S(s) = \langle d0 | s0 \rangle, S(\sigma) = \langle d0 | p0 \rangle, S(\pi) = \langle d1 | p1 \rangle$ The G_s, G_σ, G_π entries are dimensionless adjustable parameters of the model, whose values are determined from the positions of the first three absorption bands in the experimental spectrum. They can be approximated to a single value, i.e. $G_s = G_\sigma = G_\pi = G$, which then can be estimated from one (lowest in energy)

absorption band only.[1] The summation in Eq. (4) is extended only to the nearest neighbors of an impurity ion (i.e. six ligands in the case of an octahedral impurity centers formed by the Mn^{4+} ions), since the overlap with the ions from the further (second, third etc) coordination spheres can be safely neglected.

The ECM employs a small number of fitting parameters and allows for calculating the crystal field parameters and energy levels of impurities in crystals without making any assumptions about the impurity center symmetry. The reliability and vitality of the ECM is confirmed by its success in calculating the energy level of the transition metal and rare earth ions.[1-4]

In the present work the experimental structural data were used to generate clusters consisting of more than 78000 atoms, to ensure proper convergence of the crystal lattice sums. The results of CFPs calculations are shown in **Table S5**, whereas **Table S6** collects the calculated Mn^{4+} energy levels in the experimentally studied range.

The octahedral symmetry of the Mn^{4+} sites is confirmed by the structure of the crystal field Hamiltonian, in which only two CFPs B_4^4 and B_4^0 differ from zero. In addition, the degeneracy of all orbital triplet and doublet states is kept.

2. Figures

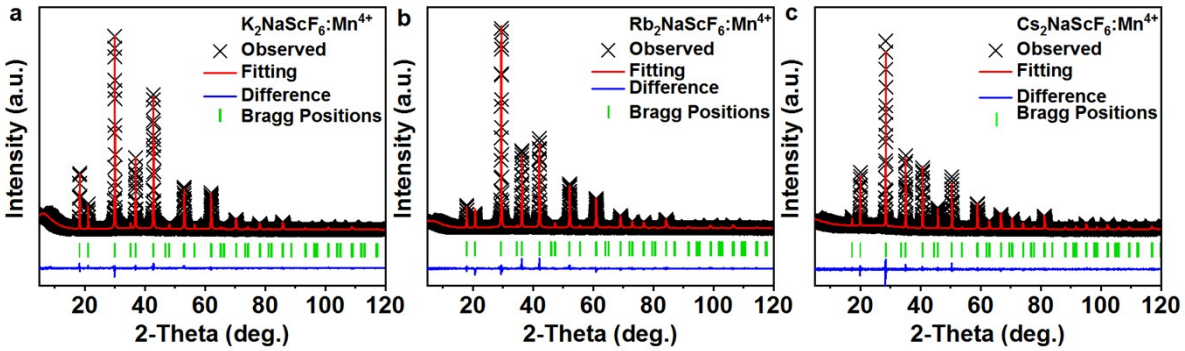

Fig. S1. XRD Rietved refinement patterns of (a) KNSF (1.30 %), (b) RNSF (1.41 %) and (c) CNSF (1.24 %) phosphors.

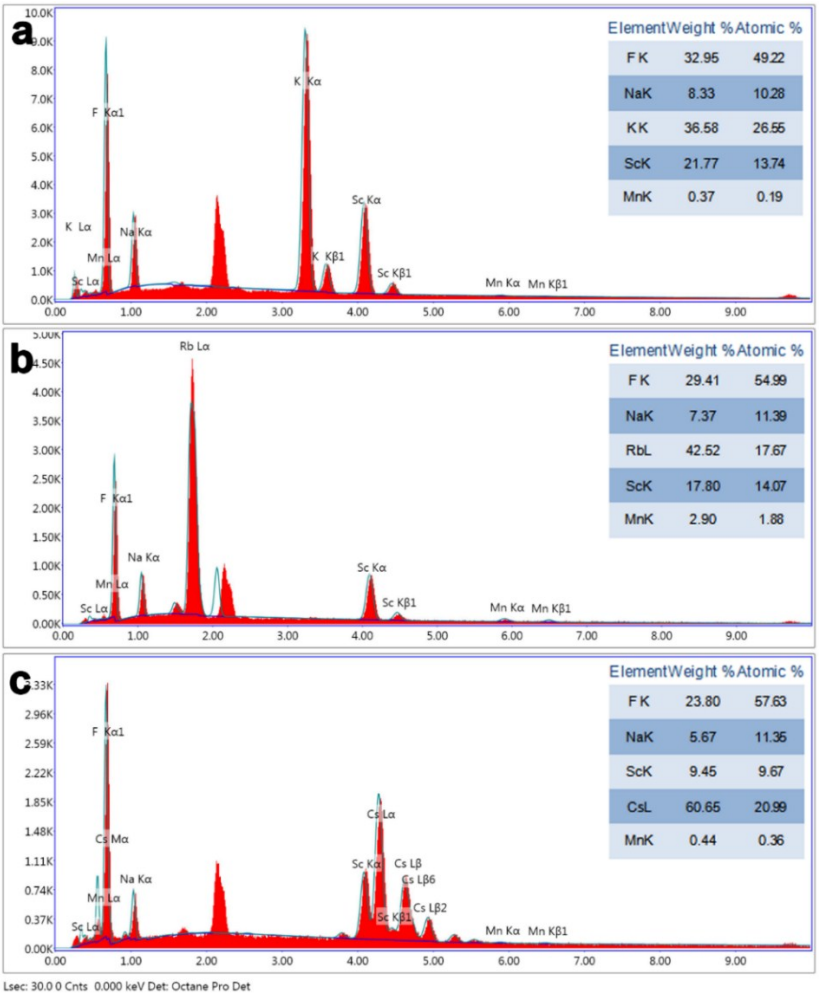

Fig. S2. EDS results of optimized (a) KNSF (1.30 %), (b) RNSF (1.41 %) and (c) CNSF (1.24 %) phosphors.

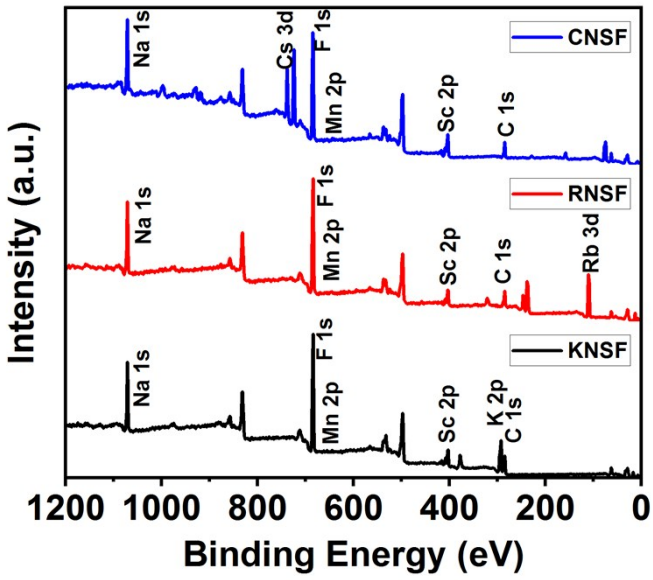

Fig. S3. XPS spectra of optimized KNSF, RNSF and CNSF phosphors.

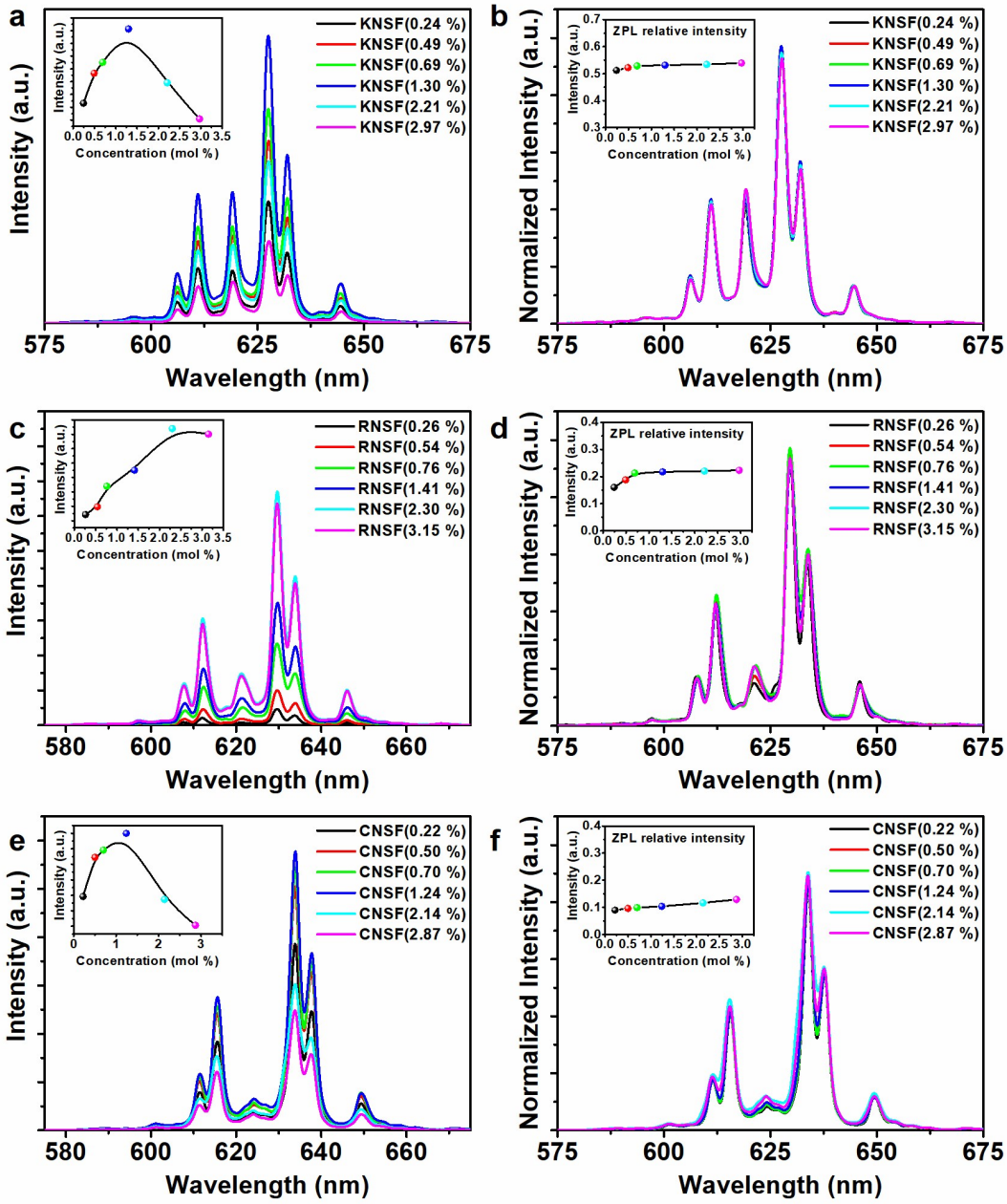

Fig. S4. PL spectra and integrated intensity (embedded Fig.) of (a) KNSF, (c) RNSF and (e) CNSF phosphors with different Mn^{4+} doping concentration, respectively. Normalized PL spectra and the changes of relative ZPL intensity (embedded Fig.) of (b) KNSF, (d) RNSF and (f) CNSF phosphors with different Mn^{4+} doping concentration, respectively.

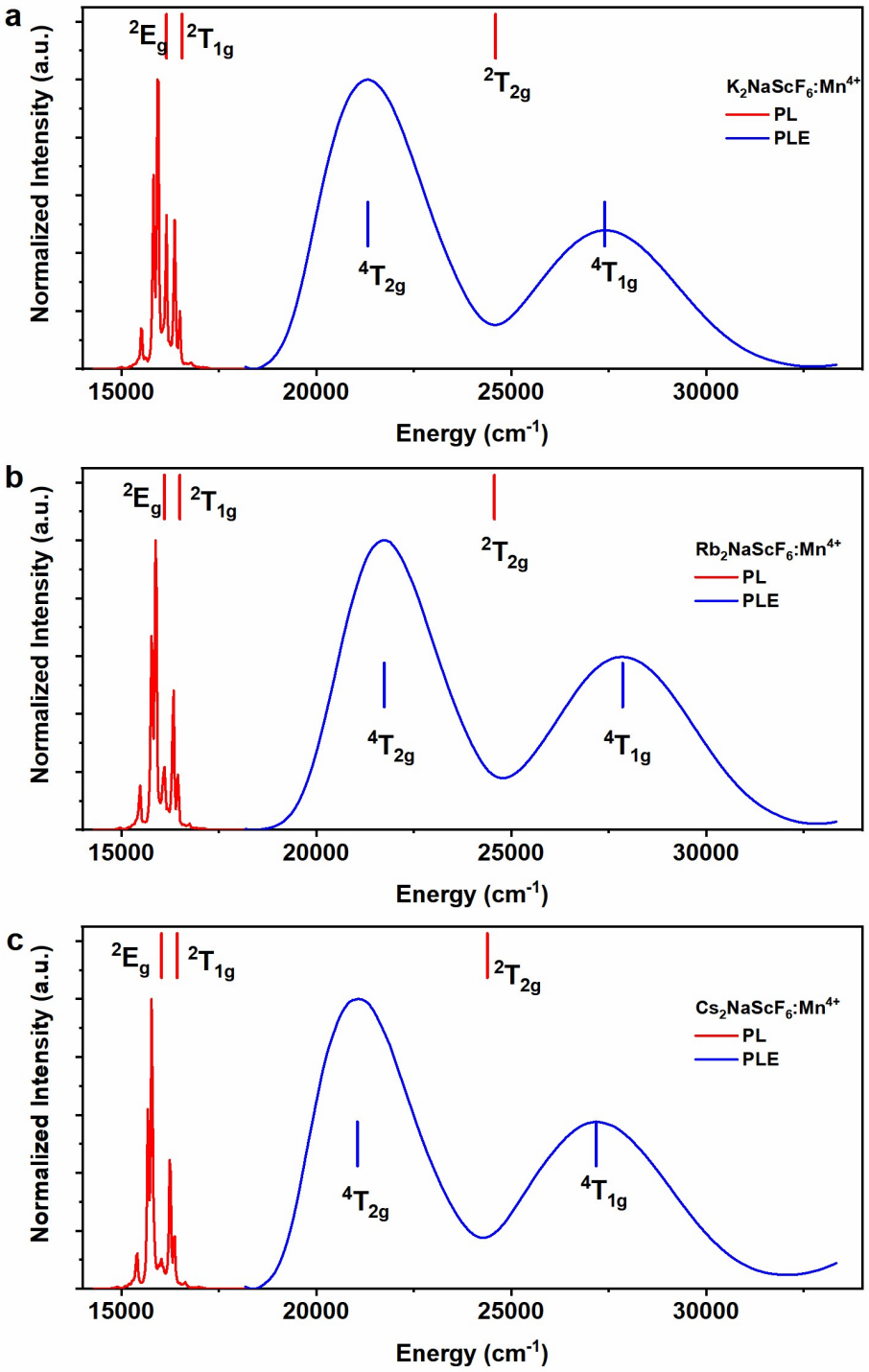

Fig. S5. Experimental excitation/emission spectra and Mn^{4+} calculated energy levels in (a) K_2NaScF_6, (b) Rb_2NaScF_6 and (c) Cs_2NaScF_6.

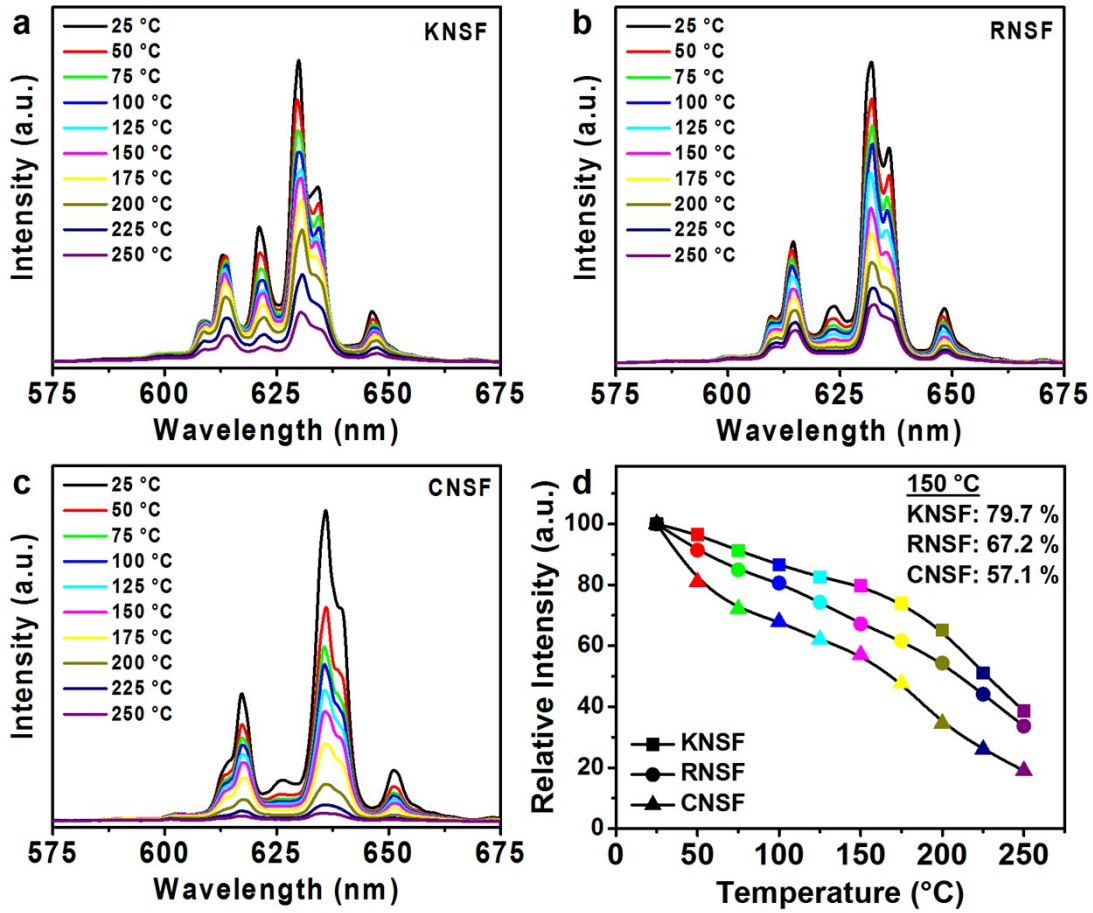

Fig. S6. Temperature-dependent PL spectra of the optimized ANSF phosphors: (a) KNSF (1.30 %), (b) RNSF (1.41 %) and (c) CNSF (1.24 %) phosphors. (d) The relative intensities of ANSF phosphors under different temperatures.

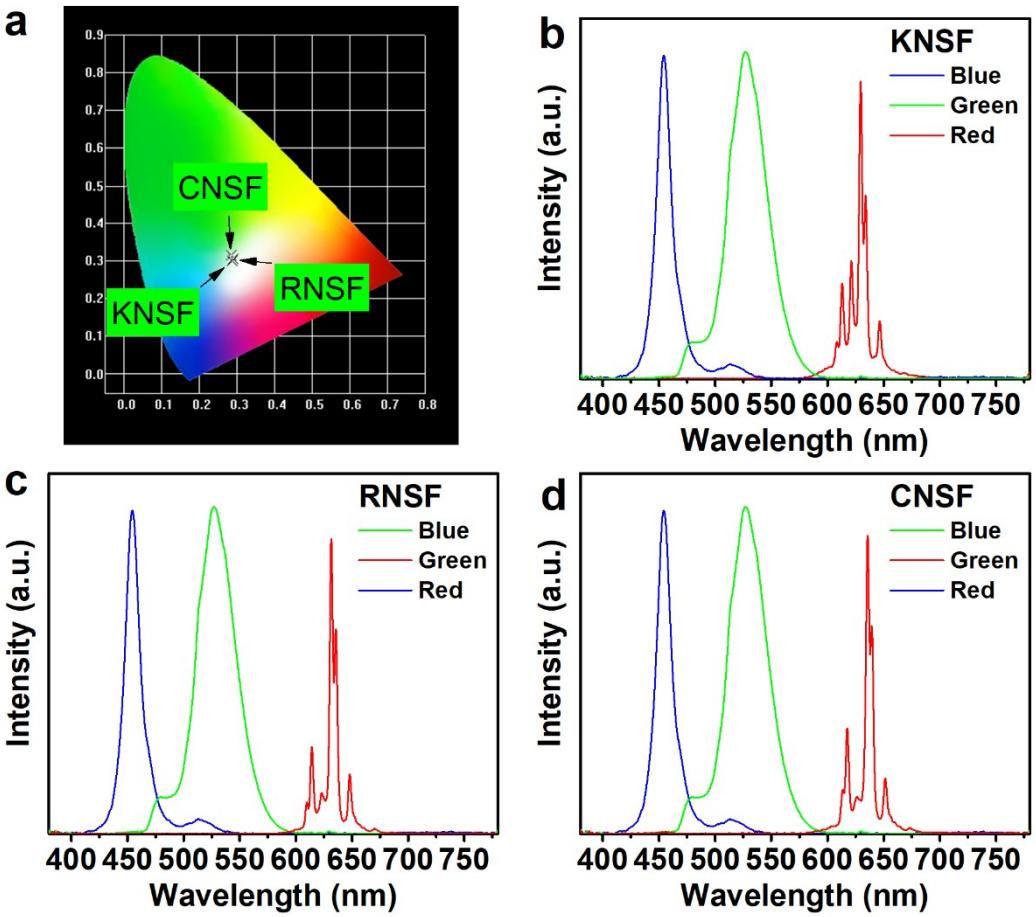

Fig. S7. (a) CIE chromaticity coordinates distribution of each WLED. RGB spectra of different WLEDs after filtered by CFs: (b) KNSF, (c) RNSF and (d) CNSF.

3. Tables

Table S1. The fluorescence lifetime and structure of typical Mn^{4+}-doped fluoride phosphors.

Phosphors	Lifetime $\tau_{1/e}$ (ms)	ZPL	Structure	Space group	conc. (mol %)	Ref.
$Na_2SiF_6:Mn^{4+}$	5.80	Strong	Trigonal	$D_3^2 - P321$	-	5
$K_2SiF_6:Mn^{4+}$	8.30	weak	Cubic	$O_h^5 - Fm\bar{3}m$	-	6
$K_3SiF_7:Mn^{4+}$	5.80	Weak	Tetragonal	P4/mbm	1	7
$Rb_2SiF_6:Mn^{4+}$	8.26	Weak	Cubic	$O_h^5 - Fm\bar{3}m$	-	8
$Rb_3SiF_7:Mn^{4+}$	5.38	Weak	Tetragonal	P4/mbm	1	7
$Cs_2SiF_6:Mn^{4+}$	7.81	Weak	Cubic	$O_h^5 - Fm\bar{3}m$	10.75	9
$Na_2GeF_6:Mn^{4+}$	6.58	Strong	Trigonal	$D_3^2 - P321$	< 10	10
$K_2GeF_6:Mn^{4+}$	6.68	Weak	Trigonal	$D_{3d}^3 - P\bar{3}m1$	< 3	10
$Rb_2GeF_6:Mn^{4+}$	6.02	Weak	Trigonal	$D_{3d}^3 - P\bar{3}m1$	< 0.8	10
$Rb_2GeF_6:Mn^{4+}$	5.8	Strong	Hexagonal	$C_{6v}^4 - P63mc$	-	11
$Cs_2GeF_6:Mn^{4+}$	7.52	Weak	Cubic	$O_h^5 - Fm\bar{3}m$	< 3	10
$K_2TiF_6:Mn^{4+}$	5.70	Weak	Trigonal	$D_{3d}^3 - P\bar{3}m1$	5.5	12
$Rb_2TiF_6:Mn^{4+}$	5.20	Weak	Trigonal	$D_{3d}^3 - P\bar{3}m1$	-	13
$Na_3AlF_6:Mn^{4+}$	4.68	Strong	Monoclinic	$C_{2h}^5 - P21/c$	1.58	14
$K_3AlF_6:Mn^{4+}$	3.50	Strong	Cubic	$O_h^5 - Fm\bar{3}m$	3.41	15
$K_2NaAlF_6:Mn^{4+}$	6.63	Strong	Cubic	$O_h^5 - Fm\bar{3}m$	2.03	16
$Cs_3AlF_6:Mn^{4+}$	2.83	Weak	Cubic	$O_h^5 - Fm\bar{3}m$	1.83	17
$K_2NaGaF_6:Mn^{4+}$	5.68	Strong	Cubic	$O_h^5 - Fm\bar{3}m$	-	18
$K_2NbF_7:Mn^{4+}$	3.7	Strong	Monoclinic	*P121*	< 1	19
$KTeF_5:Mn^{4+}$	3.29	Medium	Orthorhombic	*Pbcm*	0.23	20

$KZnF_3:Mn^{4+}$	3.43	Strong	Cubic	$O_h^5 - Fm\bar{3}m$	< 0.5	[21]
$Na_2WO_2F_4:Mn^{4+}$	1.05	Strong	Orthorhombic	*Pbcn*	< 0.5	[22]

Table S2. ICP results of Mn concentration of $A_2NaSc_{1-x}Mn_xF_6$ phosphors

Theoretical concentration (mol %)	Effective concentration (mol %)		
K_2MnF_6: $(NH_4)_3ScF_6$	$K_2NaSc_{1-x}Mn_xF_6$	$Rb_2NaSc_{1-x}Mn_xF_6$	$Cs_2NaSc_{1-x}Mn_xF_6$
0.5	0.24	0.26	0.22
1.0	0.49	0.54	0.50
1.5	0.69	0.76	0.70
3.0	1.30	1.41	1.24
5.0	2.21	2.30	2.14
7.0	2.97	3.15	2.87

Table S3. Crystallographic parameters, selected bond lengths, and bond angles from XRD Rietveld refinements of ANSF phosphors.

	KNSF (1.30 %)	RNSF (1.41 %)	CNSF (1.24 %)
Space group	$Fm\bar{3}m$	$Fm\bar{3}m$	$Fm\bar{3}m$
a = b = c (Å)	8.48482(12)	8.60713(10)	8.867(00)
α = β = γ (°)	90	90	90
Volume ($Å^3$)	610.840(27)	637.639(23)	697.15(6)
R_{wp} (%)	8.47	7.29	9.42
R_p (%)	6.83	5.58	7.59
Bond distance (Å)			
Sc–F	1.98222(3)	1.98851(3)	2.041(7)
Na-F	2.26019(4)	2.31506(3)	2.392(7)
K–F	3.00305(3)	-	-
Rb–F	-	3.04746(3)	-
Cs-F	-	-	3.1399(5)
Sc–Sc	5.99967(6)	6.08616(6)	6.2699(6)

∠ FScF (°)	90, 180	90, 180	90, 180

Table S4. EQE, IQE, and AE of optimal ANSF phosphors.

Samples	Doped concentration (mol %)	EQE (%)	IQE (%)	AE (%)
KNSF	1.30	9.09	57.13	15.91
RNSF	2.30	10.38	54.98	18.88
CNSF	1.24	10.82	51.99	20.81

Table S5. Non-zero crystal field parameters B_p^k (Stevens normalization) and Racah parameters *B*, *C* (all in cm^{-1}) for Mn^{4+} ion in KNSF, RNSF, and CNSF. The values of the ECM non-dimensional parameter *G* are also given.

	K_2NaScF_6	Rb_2NaScF_6	Cs_2NaScF_6
B_4^0	5597	5707	5526
B_4^4	27984	28533	27632
G	17.38	18.015	15.772
B	562	565	568
C	3929	3902	3874

Table S6. Calculated and experimentally observed energy levels (all in cm^{-1}) for Mn^{4+} ions in KNSF, RNSF, and CNSF.

	K_2NaScF_6		Rb_2NaScF_6		Cs_2NaScF_6	
	Exp.	Calc.	Exp.	Calc.	Exp.	Calc.
$^4A_{2g}$ (^4F)		0		0		0
^2E_g (^2G)	16155	16156	16103	16102	16026	16026
$^2T_{1g}$ (^2G)		16550		16498		16430
$^4T_{2g}$ (^4F)	21322	21321	21739	21739	21053	21053
$^2T_{2g}$ (^2G)		24594		24565		24385
$^4T_{1g}$ (^4F)	27397	27393	27855	27856	27174	27170

$^4T_{1g}$ (^4P)	44999	45838	44508

Table S7. Important experimental spectra wavelengths of ANSF phosphors

		$K_2NaScF_6:Mn^{4+}$		$Rb_2NaScF_6:Mn^{4+}$		$Cs_2NaScF_6:Mn^{4+}$	
	vibronic modes	Wavelength (nm)	Energy (cm^{-1})	Wavelength (nm)	Energy (cm^{-1})	Wavelength (nm)	Energy (cm^{-1})
Anti-Stokes emission	v_3	596	16779	597	16750	601	16639
	v_4	606	16502	608	16447	611	16367
	v_6	611	16367	612	16340	616	16234
ZPL		619	16155	621	16103	624	16026
Stokes emission	v_6	628	15924	630	15873	634	15773
	v_4	632	15823	634	15773	638	15674
	v_3	645	15504	646	15480	649	15408
$^4A_{2g}\rightarrow{}^4T_{1g}$		365	27397	359	27855	368	27174
$^4A_{2g}\rightarrow{}^4T_{2g}$		469	21322	460	21739	475	21053

Table S8. Total formation energy of two kinds of vacancy environment of Mn^{4+} substituted in a 3×1×1 supercell of ANSF.

Structure	concentration mol %	Cell	Total formation energy (eV)	
			$V_{Sc}^{'''}$	$V_{Na}^{'}$
KNSF	8.33	3×1×1	-628.71509	-634.0716
RNSF	8.33	3×1×1	-624.65489	-630.52759
CNSF	8.33	3×1×1	-621.61315	-627.73708

Table S9. Photoelectric properties of WLEDs and color gamut for LCD backlights

Phosphor		CCT	LE	Color gamut	Ref.
Green	Red	(K)	(lm/W)	(% NTSC)	
β-Sialon:Eu^{2+}	CASN:Eu^{2+}	8620	38 (20 mA)	82.1	[23]
β-Sialon:Eu^{2+}	$K_2SiF_6:Mn^{4+}$	8000	94 (120 mA)	85.9	[24]
YAG:Ce^{3+}		8000	105 (60 mA)	67.9	[25]
β-Sialon:Eu^{2+}	$K_2NbF_7:Mn^{4+}$	11338	94.68 (120 mA)	86.7	[19]

Reference

1. B. Z. Malkin, *Crystal Field and Electron-Phonon Interaction in Rare-Earth Ionic Paramagnets*, Elsevier, 1987.
2. M. G. B. Nicolae M. Avram, *Optical Properties of 3d-Ions in Crystals: Spectroscopy and Crystal Field Analysis*, Springer Berlin Heidelberg, 2013.
3. M. M. Medić, M. G. Brik, G. Dražić, Ž. M. Antić, V. M. Lojpur and M. D. Dramićanin, *J. Phys. Chem. C*, 2015, **119**, 724-730.
4. V. Đorđević, M. G. Brik, A. M. Srivastava, M. Medić, P. Vulić, E. Glais, B. Viana and M. D. Dramićanin, *Opt. Mater.*, 2017, **74**, 46-51.
5. H.-D. Nguyen, C. C. Lin, M.-H. Fang and R.-S. Liu, *J. Mater. Chem. C*, 2014, **2**, 10268-10272.
6. J. W. Moon, B. G. Min, J. S. Kim, M. S. Jang, K. M. Ok, K. Y. Han and J. S. Yoo, *Opt. Mater.*, 2016, **6**, 782-792.
7. M. Kim, W. B. Park, J. W. Lee, J. Lee, C. H. Kim, S. P. Singh and K.-S. Sohn, *Chem. Mater.*, 2018, **30**, 6936-6944.
8. M.-H. Fang, H.-D. Nguyen, C. C. Lin and R.-S. Liu, *J. Mater. Chem. C*, 2015, **3**, 7277-7280.
9. E. H. Song, Y. Y. Zhou, X. B. Yang, Z. F. Liao, W. R. Zhao, T. T. Deng, L. Y. Wang, Y. Y. Ma, S. Ye and Q. Y. Zhang, *ACS Photonics*, 2017, **4**, 2556-2565.
10. H. Z. Lian, Q. M. Huang, Y. Q. Chen, K. Li, S. S. Liang, M. M. Shang, M. M. Liu and J. Lin, *Inorg. Chem.*, 2017, **56**, 11900-11910.
11. S. Sakurai, T. Nakamura and S. Adachi, *Jpn. J. Appl. Phys.*, 2018, **57**.
12. H. M. Zhu, C. C. Lin, W. Q. Luo, S. T. Shu, Z. G. Liu, Y. S. Liu, J. T. Kong, E. Ma, Y. G. Cao, R. S. Liu and X. Y. Chen, *Nat. Commun.*, 2014, **5**, 4312.
13. S. Sakurai, T. Nakamura and S. Adachi, *ECS J. Solid State Sci. Technol.* , 2016, **5**, R206-R210.
14. E. H. Song, J. Q. Wang, S. Ye, X. F. Jiang, M. Y. Peng and Q. Y. Zhang, *J. Mater. Chem. C*, 2016, **4**, 2480-2487.
15. E. H. Song, J. Q. Wang, J. H. Shi, T. T. Deng, S. Ye, M. Y. Peng, J. Wang, L. Wondraczek and Q. Y. Zhang, *ACS Appl. Mater. Inter.*, 2017, **9**, 8805-8812.
16. L. Y. Wang, E. H. Song, T. T. Deng, Y. Y. Zhou, Z. F. Liao, W. R. Zhao, B. Zhou and Q. Y. Zhang, *Dalton. Trans.*, 2017, **46**, 9925-9933.
17. H. Ming, J. Zhang, L. Liu, J. Peng, F. Du and X. Ye, *ECS J. Solid State Sci. Technol.* , 2018, **7**, R149-R155.
18. C. Y. Jiang, M. G. Brik, L. H. Li, L. Y. Li, J. Peng, J. N. Wu, M. S. Molokeev, K. L. Wong and M. Y. Peng, *J. Mater. Chem. C*, 2018, **6**, 3016-3025.
19. H. Lin, T. Hu, Q. Huang, Y. Cheng, B. Wang, J. Xu, J. Wang and Y. Wang, *Laser Photonics Rev.*, 2017, **11**, 1700148.
20. T. T. Deng, E. H. Song, J. Su, Y. Y. Zhou, L. Y. Wang, S. Ye and Q. Y. Zhang, *J. Mater. Chem. C*, 2018, **6**, 4418-4426.
21. T. Hu, H. Lin, F. Lin, Y. Gao, Y. Cheng, J. Xu and Y. Wang, *J. Mater. Chem. C*, 2018, **6**, 10845-10854.
22. T. Hu, H. Lin, Y. Gao, J. Xu, J. Wang, X. Xiang and Y. Wang, *J. Am. Ceram. Soc.*, 2018, **101**, 3437-3442.

23. R. J. Xie, N. Hirosaki and T. Takeda, *Appl Phys Express*, 2009, **2**, 022401-022401-022403.
24. L. Wang, X. Wang, T. Kohsei, K. Yoshimura, M. Izumi, N. Hirosaki and R. J. Xie, *Opt. Express*, 2015, **23**, 28707-28717.
25. J. H. Oh, H. Kang, M. Ko and Y. R. Do, *Opt. Express*, 2015, **23**, A791-804.